

 Open access • Journal Article • DOI:10.1088/0004-637X/807/2/115

The History of R-Process Enrichment in the Milky Way — [Source link](#)

[Sijing Shen](#), [Sijing Shen](#), [Ryan Cooke](#), [Enrico Ramirez-Ruiz](#) ...+3 more authors

Institutions: [University of California, Santa Cruz](#), [University of Cambridge](#), [University of Zurich](#)

Published on: 07 Jul 2015 - [The Astrophysical Journal](#) (IOP Publishing)

Topics: [Galaxy](#), [Galaxy formation and evolution](#), [Milky Way](#), [Metallicity](#) and [Eris](#)

Related papers:

- [Galactic r-process enrichment by neutron star mergers in cosmological simulations of a Milky Way-mass galaxy](#)
- [Neutron star mergers versus core-collapse supernovae as dominant r-process sites in the early Galaxy](#)
- [Production of all the r-process nuclides in the dynamical ejecta of neutron star mergers](#)
- [r-Process in Neutron Star Mergers](#)
- [Galactic evolution of rapid neutron capture process abundances: the inhomogeneous approach](#)

Share this paper:    

View more about this paper here: <https://typeset.io/papers/the-history-of-r-process-enrichment-in-the-milky-way-38ksbjh3u>



University of
Zurich^{UZH}

Zurich Open Repository and
Archive

University of Zurich
University Library
Strickhofstrasse 39
CH-8057 Zurich
www.zora.uzh.ch

Year: 2015

The history of r -process enrichment in the Milky Way

Shen, Sijing ; Cooke, Ryan J ; Ramirez-Ruiz, Enrico ; Madau, Piero ; Mayer, Lucio ; Guedes, Javiera

Abstract: We investigate the production sites and the enrichment history of r -process elements in the Galaxy, as traced by the [Eu/Fe] ratio, using the high resolution, cosmological zoom-in simulation 'Eris'. At $z = 0$, Eris represents a close analog to the Milky Way, making it the ideal laboratory to understand the chemical evolution of our Galaxy. Eris formally traces the production of oxygen and iron due to Type-Ia and Type-II supernovae. We include in post-processing the production of r -process elements from compact binary mergers. Unlike previous studies, we find that the nucleosynthetic products from compact binary mergers can be incorporated into stars of very low metallicity and at early times, even with a minimum delay time of 100 Myr. This conclusion is relatively insensitive to modest variations in the merger rate, minimum delay time, and the delay time distribution. By implementing a first-order prescription for metal-mixing, we can further improve the agreement between our model and the data for the chemical evolution of both $[\alpha/\text{Fe}]$ and [Eu/Fe]. We argue that compact binary mergers could be the dominant source of r -process nucleosynthesis in the Galaxy.

DOI: <https://doi.org/10.1088/0004-637X/807/2/115>

Posted at the Zurich Open Repository and Archive, University of Zurich

ZORA URL: <https://doi.org/10.5167/uzh-121971>

Journal Article

Accepted Version

Originally published at:

Shen, Sijing; Cooke, Ryan J; Ramirez-Ruiz, Enrico; Madau, Piero; Mayer, Lucio; Guedes, Javiera (2015).

The history of r -process enrichment in the Milky Way. *The Astrophysical Journal*, 807(2):115.

DOI: <https://doi.org/10.1088/0004-637X/807/2/115>

THE HISTORY OF R-PROCESS ENRICHMENT IN THE MILKY WAY

SIJING SHEN¹, RYAN J. COOKE², ENRICO RAMIREZ-RUIZ², PIERO MADAU², LUCIO MAYER³ AND JAVIERA GUEDES⁴

Draft version April 10, 2015

ABSTRACT

We investigate the production sites and the enrichment history of r -process elements in the Galaxy, as traced by the [Eu/Fe] ratio, using the high resolution, cosmological zoom-in simulation ‘Eris’. At $z = 0$, Eris represents a close analog to the Milky Way, making it the ideal laboratory to understand the chemical evolution of our Galaxy. Eris formally traces the production of oxygen and iron due to Type-Ia and Type-II supernovae. We include in post-processing the production of r -process elements from compact binary mergers. Unlike previous studies, we find that the nucleosynthetic products from compact binary mergers can be incorporated into stars of very low metallicity and at early times, even with a minimum delay time of 100 Myr. This conclusion is relatively insensitive to modest variations in the merger rate, minimum delay time, and the delay time distribution. By implementing a first-order prescription for metal-mixing, we can further improve the agreement between our model and the data for the chemical evolution of both $[\alpha/\text{Fe}]$ and [Eu/Fe]. We argue that compact binary mergers could be the dominant source of r -process nucleosynthesis in the Galaxy.

Subject headings: stars: abundances — Galaxy: abundances — Galaxy: evolution — methods: numerical

1. INTRODUCTION

The chemical abundance patterns of Galactic halo stars encode precious information about the various stellar progenitor systems that existed prior to their birth. These ancient halo stars therefore provide an insight into the nucleosynthesis processes that occurred early in the history of the Milky Way. Of particular interest in this regard is the heavy element composition of Galactic halo stars (Truran et al. 2002; Cowan & Sneden 2006). For stars with an [Fe/H] metallicity in the range $\approx 10^{-2}$ to $\approx 10^{-3}$ solar, elements in the mass region above Ba have been found to be consistent with enrichment by a pure r -process with a distribution that is characteristic of solar system matter but with a large star-to-star bulk scatter in their concentrations with respect to the lighter elements such as Mg (Sneden, Cowan, & Gallino 2008). The presence of these heavy nuclei in such primitive stars demonstrates that the r -process has operated in a fairly robust manner over large periods of time in Galactic history, while the large dispersion in their abundance relative to lighter nuclei suggests an early, chemically unmixed and inhomogeneous Milky Way (Fields et al. 2002). At later times, these localized inhomogeneities would be smoothed out as subsequent events take place and heavy element products are given more time to migrate throughout the Galaxy (Travaglio et al. 2001).

Nucleosynthesis theory has identified the specific physical conditions and nuclear properties required for the r -process (Burbidge et al. 1957). However, the astrophysical site for this process has not been unambiguously identified. The original work on this subject suggested that the neutron-rich regions outside a nascent neutron star in a Type II supernova (Woosley et al. 1994; Takahashi et al. 1994) or the ejecta from the last seconds of a merger between a neutron star (NS) and a compact binary companion are the most likely for-

mation sites (Lattimer et al. 1977; Freiburghaus et al. 1999). Compact mergers involving a neutron star are much rarer than SN II (Cowan & Thielemann 2004) and should occur far from their birth sites (e.g. Kelley et al. 2010). Furthermore, these two mechanisms eject different quantities of r -process material. These differences should surely be imprinted in the enrichment pattern of r -process elements and may ultimately identify the dominant production mechanism (Argast et al. 2004; Matteucci et al. 2014; Cescutti et al. 2013; Tsujimoto & Shigeyama 2014; Cescutti & Chiappini 2014).

The build-up of the elements in our Galaxy, including that of the r -process, can be studied in detail by using realistic galactic chemical evolution (GCE) models (e.g. Pagel 2009). 3D hydrodynamic simulations that incorporate the details of chemical evolution (often referred to as chemodynamical simulations) have been widely used in the literature to study the enrichment history and distribution of various elements in galaxies (e.g. Kawata & Gibson 2003; Kobayashi & Nakasato 2011; Rahimi et al. 2011; Few et al. 2012; Pilkington et al. 2012; Minchev et al. 2013; Brook et al. 2014; Few et al. 2014). Because such simulations follow the dynamics and chemical evolution self-consistently, they are better equipped to address the inhomogeneous enrichment of the ISM and the mixing of metals. In addition, simulations performed in a cosmological context (e.g., Kobayashi & Nakasato 2011; Rahimi et al. 2011; Pilkington et al. 2012; Brook et al. 2014; Few et al. 2014) are able to capture the larger scale mixing mechanisms including gas inflows, satellite mergers, galactic winds and fountains, and instabilities in rotationally supported disks, all of which are undoubtedly important to understand the enrichment and dispersal of heavy elements. On the other hand, since cosmological simulations today are limited by resolutions of a few tens to hundreds of parsecs, they inevitably involve “sub-grid” models for star formation, stellar feedback, and/or turbulent mixing. As such, large uncertainties still exist at the hundred parsec scale. Investigating the distribution of chemical elements in these simulations and comparing them extensively with the observational data can, in turn, provide important constraints on these sub-resolution

¹ Institute of Astronomy, University of Cambridge, Madingley Road, Cambridge, CB3 0HA, United Kingdom

² Department of Astronomy and Astrophysics, University of California, 1156 High Street, Santa Cruz, CA 95064, USA

³ Institute of Theoretical Physics, University of Zürich, Winterthurerstrasse 190, CH-9057 Zürich, Switzerland

⁴ Teralytics AG, Zollstrasse 62, 8005 Zürich, Switzerland

models and improve the modeling of astrophysical fluids.

The origin and evolution of the r -process elements, however, are mostly addressed using analytical or semi-analytical models (e.g. Argast et al. 2004; Matteucci et al. 2014; Cescutti et al. 2013; Tsujimoto & Shigeyama 2014; Cescutti & Chiappini 2014; although see van de Voort et al. 2015), possibly because most simulations have not implemented the production of r -process elements due to their uncertain origins described above. In this Paper we employ Eris, one of the highest resolution cosmological simulations of the formation of a Milky Way-size galaxy (Guedes et al. 2011), to investigate the synthesis of the heavy r -process elements in our Galaxy, as traced by the [Eu/Fe] ratio.

2. METHODS

2.1. The Eris Simulation

We use the high resolution, zoom-in cosmological simulation of a Milky Way Galaxy analog “Eris” to track the production and transportation of r -process elements. A detailed description of the Eris simulation is provided by Guedes et al. (2011). Here we briefly outline the aspects relevant to this study. The simulation was performed with the parallel TreeSPH code GASOLINE (Wadsley, Stadel, & Quinn 2004) in a *WMAP-3* cosmology. The run includes a uniform UV background (Haardt & Madau 1996), Compton cooling, atomic cooling and metallicity dependent radiative cooling at $T < 10^4$ K. Star formation is modelled by stochastically forming “star particles” out of gas that is sufficiently cold ($T < 3 \times 10^4$ K) and reaches a threshold density of $n_{\text{SF}} = 5$ atoms cm^{-3} . The local star formation rate follows $d\rho_*/dt = 0.1\rho_{\text{gas}}/t_{\text{dyn}} \propto \rho_{\text{gas}}^{1.5}$, where ρ_* and ρ_{gas} are the stellar and gas densities, respectively, and t_{dyn} is the local dynamical time. Each star particle has initial mass $m_* = 6000 M_{\odot}$ and represents a simple stellar population that follows a Kroupa, Tout, & Gilmore (1993) initial mass function (IMF), and inherits the metallicity of its parent gas particle. Star particles inject energy, mass and metals back into the ISM through Type Ia, Type II SNe and stellar winds (Stinson et al. 2006). Eris’ high resolution enables the development of an inhomogeneous ISM which allows realistic clustered star formation and strong cumulative feedback from coeval supernova explosions. Large scale galactic winds are launched as a consequence of stellar feedback, which transports a substantial quantity of metals into the circumgalactic medium and enriches the subsequent gas accretion (Shen et al. 2013). At $z = 0$, Eris forms an extended, rotationally supported stellar disk with a small bulge-to-disk ratio. The structural properties, the mass budget in various components and the scaling relations in Eris are simultaneously consistent with observations of the Galaxy (Guedes et al. 2011).

The simulation follows Raiteri, Villata, & Navarro (1996) to model metal enrichment from SN II and SN Ia. Metals are distributed to gas within the SPH smoothing kernel (which consists of 32 neighboring particles). For SN II, metals are released as the main sequence progenitors die, and iron and oxygen are produced according to the following fits to the Woosley & Weaver (1995) yields:

$$M_{\text{Fe}} = 2.802 \times 10^{-4} \left(\frac{m_*}{M_{\odot}} \right)^{1.864} M_{\odot}, \quad (1)$$

and

$$M_{\text{O}} = 4.586 \times 10^{-4} \left(\frac{m_*}{M_{\odot}} \right)^{2.721} M_{\odot}. \quad (2)$$

For SN Ia, each explosion produces $0.63 M_{\odot}$ of iron and $0.13 M_{\odot}$ of oxygen (Thielemann, Nomoto, & Yokoi 1986). Stellar wind feedback is based on Kennicutt, Tamblyn, & Congdon (1994), and the returned mass fraction was determined following Weidemann (1987). The returned gas inherits the metallicity of the star particle. We adopt the Asplund et al. (2009) solar abundance scale for elements other than O and Fe, that are not tracked in the simulation.

We note that there are several limitations to our modeling. First, because the smallest gas resolution element is an ensemble of gas particles within the smoothing kernel rather than individual particles, forcing the newly-formed star particle to inherit metallicity only from its parent gas particle may amplify sub-resolution metallicity variances between gas particles. Second, the simulation used a traditional SPH formalism where metals advect with the fluid perfectly, without mixing due to microscopic motions (such as turbulence). Both caveats may cause an artificially inhomogeneous chemical distribution (Wiersma et al. 2009; Shen, Wadsley, & Stinson 2010). While improved runs within the Eris suite include a model for turbulent diffusion (Shen et al. 2013), for this study we have used a simulation without mixing so that our r -process injection method is consistent with the production and distribution of O and Fe in the simulation. In Section 3, we explore a simple diffusion model to illustrate the effect of mixing. Instead of using the metallicity of the parent gas particle, we average the metallicity over 128 neighboring gas particles to determine the metallicity of the newly-formed star particle.

In addition, despite being one of the highest resolution galaxy formation simulations that evolves to $z = 0$, our model still lacks the spatial and temporal resolution to correctly follow the formation and enrichment of the first generation of Population III stars as well as early Population II stars. It is a common practice in the literature to introduce a metallicity “floor” at high redshift to account for the unresolved earliest population (e.g., Krumholz & Gnedin 2011; Kuhlen et al. 2013; Hopkins et al. 2014). The floor metallicity is typically around 10^{-4} to $10^{-3} Z_{\odot}$, motivated by detailed simulations of Population III star formation and primordial metal enrichment (e.g. Wise et al. 2012). Although a metallicity floor was not included in Eris during the run, in Section 3 we investigate the affect of a modest metallicity floor ($10^{-4} Z_{\odot}$) implemented in post-processing. This is achieved by assigning a minimum abundance of [Fe/H] = -4.0 to every gas particle, and an α -enhancement of [O/Fe] +0.4, corresponding to the IMF-weighted alpha-enhancement estimated from models of zero-metallicity stellar nucleosynthesis (Woosley & Weaver 1995; Heger & Woosley 2010; Limongi & Chieffi 2012).

2.2. R-Process Production Sites and Injection History

The key ingredient in our analysis is the realistic star formation history (SFH) of a galaxy simulated in a cosmological context which at redshift $z = 0$ is a close analog of the Milky Way (Guedes et al. 2011). In this section we describe our post-processing implementation for NS mergers. The important elements of our model include: (1) The delay-time distribution (DTD) of mergers; (2) the merger rate and the yield of r -process elements; and (3) the spatial distribution of injection sites and their sphere of influence.

2.2.1. Delay-time distribution, merger rates and r -process yields

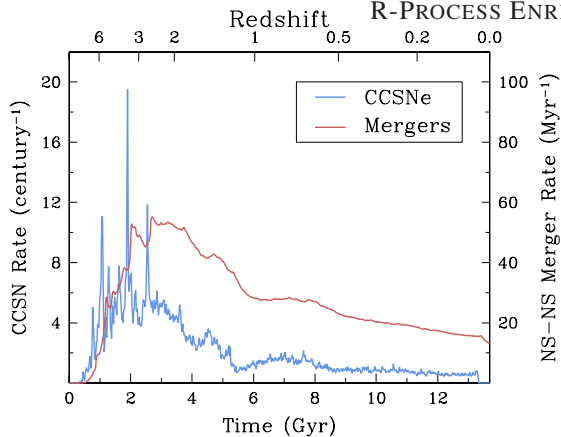


FIG. 1.— The SN II rate (blue curve, left axis), which closely traces the SFR, is compared with the NS merger rate derived from the Eris SFR and the DTD (red curve, right axis).

The merger DTD, $P(t)$, is well-modeled by a power-law (Piran 1992; Kalogera et al. 2001), although there is significant uncertainty on the value of the exponent (e.g. Behroozi et al. 2014, and references therein). Herein, we adopt $P(t) \propto t^{-n}$ for $t > t_{\text{cut}}$ and zero probability otherwise, where t_{cut} is the initial time delay after a burst of star formation before the first merger occurs. Herein we consider two power-law indices, $n = 2$ and $n = 1$, and assume conservative values of $t_{\text{cut}} = 100$ Myr and $t_{\text{cut}} = 200$ Myr (Fryer et al. 1999; Belczynski et al. 2006).

Our fiducial model assumes that each merger event produces a mass $M_{\text{tp}} = 0.05 M_{\odot}$ of r -process elements (e.g. Just et al. 2014). We also consider a model where $M_{\text{tp}} = 0.01 M_{\odot}$ is produced, which reflects the mass of dynamically ejected material (Lattimer & Schramm 1974; Rosswog et al. 1999; Metzger et al. 2010; Roberts et al. 2011; Bauswein et al. 2013; Grossman et al. 2014; Ramirez-Ruiz et al. 2014). For each merger event, we track the production of europium, which we assume is produced in solar relative proportions such that $M_{\text{Eu}}/M_{\text{tp}} = 9.3 \times 10^{-4}$ (Snedden, Cowan, & Gallino 2008).

The NS merger rate is then determined by convolving the SFH extracted from the simulation with the DTD:

$$\mathcal{R}(t) = A \int_{t_{\text{cut}}}^{t_H} \dot{M}_*(t-\tau) P(\tau) d\tau \quad (3)$$

where A is a constant that is fixed by the total number of merger events, \dot{M}_* is the star formation rate (SFR) and t_H is the Hubble time. To calculate A , we impose that the abundance of Eu/O in the final simulation output corresponds to the solar value (i.e. $[\text{Eu}/\text{O}] = 0.0$). There are ~ 260 million massive stars formed in Eris that end their life as a Type II SN, and the IMF-weighted O yield per Type II SN event is $\simeq 1 M_{\odot}$ in our model. Assuming a solar number ratio, $\log(\text{Eu}/\text{O})_{\odot} = -8.14$, the total mass of Eu needed to obtain the solar $[\text{Eu}/\text{O}]$ abundance is $\sim 18 M_{\odot}$. Thus, the total mass of r -process elements produced during the chemical evolution of Eris needs to be $18800 M_{\odot}$. If we now assume that each compact binary merger contributes $M_{\text{tp}} = 0.05 M_{\odot}$ ($0.01 M_{\odot}$) of r -process, then we require $\approx 3.76 \times 10^5$ (1.88×10^6) mergers in 13.8 Gyr to explain the observed solar Eu/O ratio. The constant A is therefore fixed by requiring that the integral of the merger rate (Eq. 3) over the lifetime of Eris is equal to 3.76×10^5 (1.88×10^6). The resulting NS merger history is shown in Figure 1 as the solid red curve, for $M_{\text{tp}} = 0.05 M_{\odot}$, which is in good agreement with the expected rates calculated

by Abadie et al. (2010). For reference, we also present the Eris SN II rate as a function of time as the blue curve in Figure 1.

2.2.2. Injection History

Compact binary mergers are expected to predominantly occur within $\sim 10 - 100$ kpc of a Milky Way-like host galaxy (Bloom, Sigurdsson, & Pols 1999; Belczynski et al. 2006; Kelley et al. 2010). Therefore, the spatial distribution of NS mergers broadly follows the stellar distribution of the host galaxy. We have thus adopted a post-processing implementation to include NS mergers in Eris. Our approach is justified since the momentum imparted to the surrounding gas by a merger is much less than that of a SN explosion, despite releasing an energy that is similar in magnitude to a SN. The gas dynamics is therefore largely unchanged.

In the top-left panel of Figure 2, we present a face-on illustration of the projected surface mass density of Eris' stars at redshift $z = 2$. By construction, this panel represents the distribution of merger injection sites. Similarly, in the top-right panel of this figure, we present the SFR surface density, which traces SN II. In the bottom panels of Figure 2, we show the surface mass density of gas on two different spatial scales, which are enriched by these events and later form a new generation of stars.

Using the above formalism, we calculate the number of NS mergers that occur between adjacent timesteps and randomly select a corresponding number of star particles from a uniform distribution to act as the merger injection sites. The surrounding gas particles are then enriched with a total Eu mass $M_{\text{Eu}}^{\text{tot}} = 4.65 \times 10^{-5} M_{\odot}$ (corresponding to $M_{\text{tp}} = 0.05 M_{\odot}$), which is distributed over the 32 neighboring gas particles according to the smoothing kernel, as outlined in Wadsley, Stadel, & Quinn (2004). We note that the oxygen and iron enrichment follow an identical scheme. The evolution of each gas particle is tracked for subsequent timesteps. When a stellar particle is born in the non-diffusion case, it inherits the Eu/Fe ratio from the parent gas particle. In our simple mixing model, the stellar particle inherits the average abundance of Eu, O and Fe from 128 neighbouring gas particles as described in Section 2.1. Hereafter, when comparing with observations, we only consider star particles present in the $z = 0$ snapshot.

3. R-PROCESS ENRICHMENT IN THE MILKY WAY

Our baseline set of model parameters include: an r -process mass of $M_{\text{tp}} = 0.05 M_{\odot}$ ejected per event, a merger DTD that has a minimum merger delay-time of $t_{\text{cut}} = 100$ Myr and a power law of the form t^{-1} , a mixing length corresponding to the 128 nearest neighbors, and an alpha-enhanced ($[\alpha/\text{Fe}] = +0.40$) metallicity floor of $[\text{Fe}/\text{H}] = -4.0$. Hereafter, we refer to this set of parameters as our fiducial model.

We now investigate the chemical evolution of the α (traced by O), Fe and r -process elements in Eris. The top-left panel of Figure 3 displays the $[\alpha/\text{Fe}]$ abundance for a representative sample (1:1000) of Eris star particles in the $z = 0$ snapshot as a function of their formation time. Although most stars exhibit super-solar $[\alpha/\text{Fe}]$ values, there are a non-negligible number of stars with strongly sub-solar values. This effect is more pronounced at the lowest metallicity, as shown in the bottom-left panel of Figure 3, where the distribution of $[\alpha/\text{Fe}]$ values is represented by dark and light green contours that respectively enclose 68 and 95 per cent of the Eris stars at a given

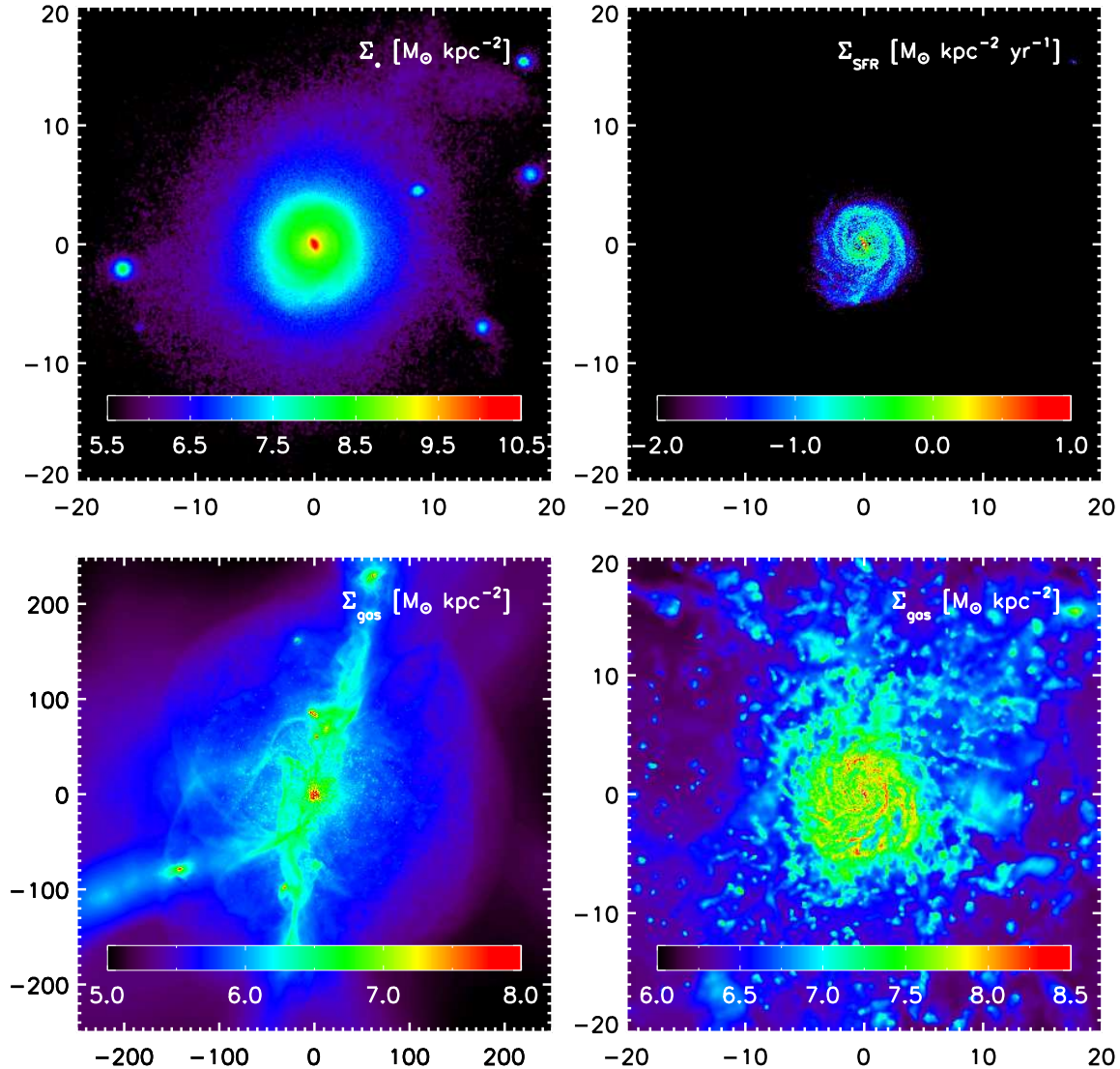


FIG. 2.— A face-on illustration of the projected surface mass density of stars (top-left panel), SFR surface density (top-right panel) and gas in different scales (bottom panels) for Eris at redshift $z = 2$. The units of all axes are in kpc.

metallicity. When $[\text{Fe}/\text{H}] \lesssim -1.5$, the $[\alpha/\text{Fe}]$ distribution bifurcates into a high and low $[\alpha/\text{Fe}]$ channel. The low $[\alpha/\text{Fe}]$ channel corresponds to star particles predominantly enriched by SN Ia (which, in our implementation, produce an O mass that is five times less than the Fe mass), whereas the high $[\alpha/\text{Fe}]$ channel represents the star particles enriched solely by SN II.

To compare with observations, we overplot a sample of $[\alpha/\text{Fe}]$ measurements for Milky Way thin disk, thick disk, and halo stars (Fulbright 2000; Reddy et al. 2003; Cayrel et al. 2004; Cohen et al. 2004; Simmerer et al. 2004; Venn et al. 2004; Barklem et al. 2005; Reddy et al. 2006; Mishenina et al. 2013; Roederer et al. 2014). We divide the observational sample into stars where α (typically Mg, Si, Ca), Fe, and Eu are *all* measured (blue symbols), and stars where only α and Fe are measured (orange symbols). Overall, there is a reasonable agreement between the observations and the upper envelope of the simulated stars. Moreover, the ‘knee’ in the α/Fe ratio near a metallicity $[\text{Fe}/\text{H}] \simeq -1.0$, which marks the increased contribution of SN Ia (e.g. Tinsley 1979), is well-reproduced by the Eris simulation.

The discrepancy between Eris and the observations at low metallicity is the result of gas particles being predominantly enriched by SN Ia, and illustrates a limitation of the traditional SPH formalism; once a gas particle is enriched with metals, it cannot share its metals with neighboring particles. Many techniques have been developed to incorporate metal diffusion in simulations, using either subgrid turbulent diffusion models (Greif et al. 2009; Shen, Wadsley, & Stinson 2010), or simply smoothing the metals within the SPH kernel (Wiersma et al. 2009). Our goal is to provide a simple demonstration of the importance of metal diffusion for studying chemical evolution. We have therefore post-processed Eris to include a metallicity floor (as described in Section 2.1) and we paint newly formed star particles with a metallicity corresponding to the mass-weighted average of the 128 nearest neighbors. The choice of 128 is based on the following estimation: At our star formation threshold density of 5 atoms cm^{-3} , this corresponds to a size that the gas can cross within the free-fall time, assuming the typical velocity dispersion of the molecular cloud. The corresponding mixing length of 128 particles peaks around 50–120 pc at all redshifts. Only in very rare

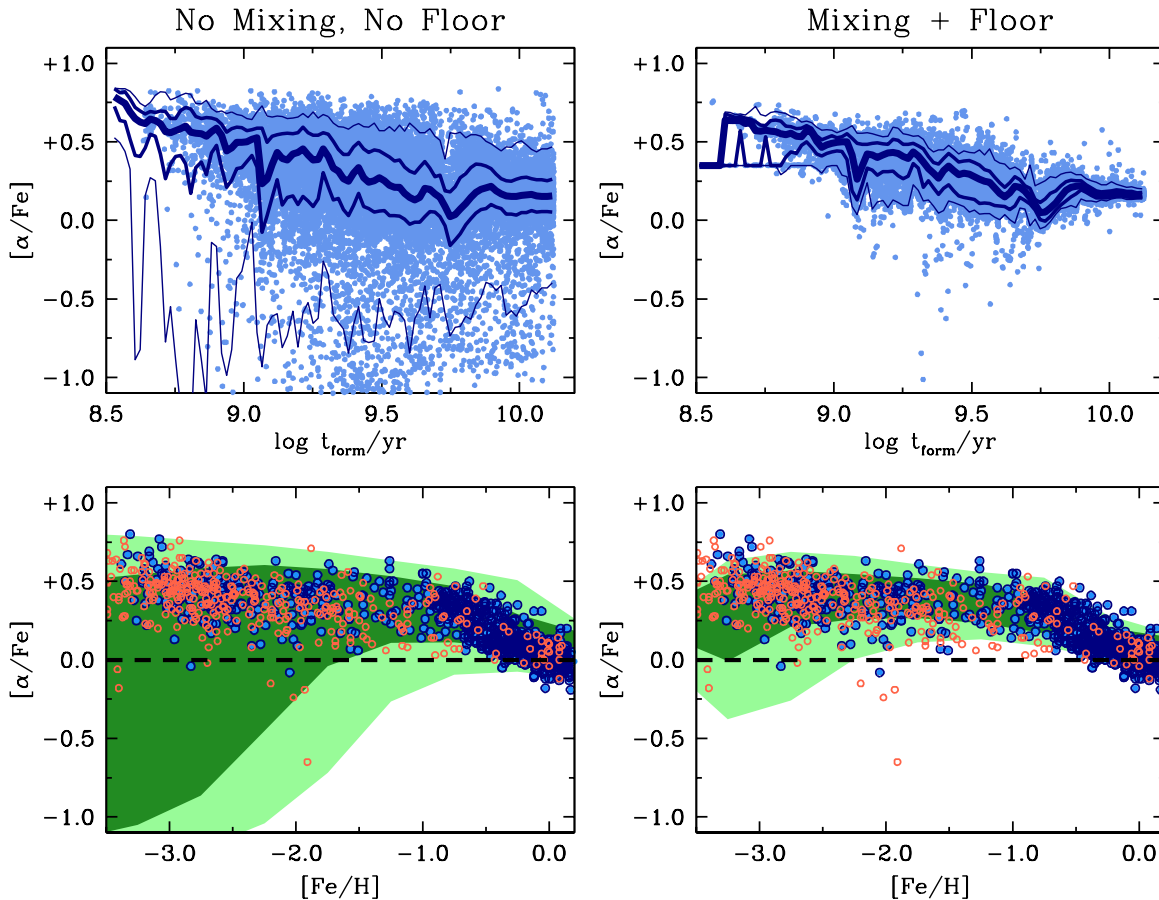


FIG. 3.— *Top panels:* The chemical evolution of O and Fe for a representative sample (1:1000) of Eris’ $z = 0$ star particles (blue symbols) as a function of the formation time. The centroid of the distribution is shown by the solid dark blue line, whilst the thinner lines enclose 68 and 95 per cent of the stars. The top-left displays the raw simulation output, without a metallicity floor and without a prescription for metal diffusion. The ‘excess’ scatter at low $[\alpha/\text{Fe}]$ is reduced considerably when we include a simple physical model for metal diffusion and a metallicity floor, as shown in the top-right panel (see text for further details). *Bottom panels:* The dark and light green contours show the $[\alpha/\text{Fe}]$ distributions that respectively enclose 68 and 95 per cent of Eris’ $z = 0$ star particles. The observational data are represented by blue symbols for stars where α , Fe, and Eu were all measured, or by orange circles when only α and Fe are reported. The dashed line represents the solar value. Our simple mixing prescription and introducing a metallicity floor of $Z = 10^{-4} Z_{\odot}$ significantly improves the agreement with the observational data.

cases (~ 2 per cent) does the mixing length exceed 500 pc. Even at high redshift (e.g. $z > 5$) where the main host progenitor undergoes vigorous mergers, less than 10 per cent of cases have a mixing length in excess of 350 pc. We have carried out a test run in which we remove all cases with smoothing length larger than 350 pc, and find that the results are essentially unchanged. The chemical evolution of $[\alpha/\text{Fe}]$ for our mixing prescription is presented in the right panels of Fig. 3, where the excess $[\alpha/\text{Fe}]$ scatter for the Eris star particles is considerably reduced at all times. The data are brought into much better agreement with the simulations at low metallicity. We emphasise that this simple model of metal diffusion is designed to illustrate the importance of subgrid mixing. Although our choice of the number of smoothing neighbours (or length) is physically motivated, 128 neighbours also provides the closest match to the observed alpha/Fe scatter seen in the simulations. In other words, we have reduced the artificial inhomogeneity in our simulation and require that our model matches the chemical evolution of α/Fe .

Using the techniques described in Section 2.2, a sample of stars enriched with the r -process in Eris are shown in the top two panels of Figure 4, assuming that the only production channel for the r -process is compact binary mergers. The left panels of Figure 4 show the results of our simulation without metal diffusion and with no metallicity floor, whereas the

right panels show our fiducial model, which contains a simple physically motivated prescription for the metal mixing, and a metallicity floor. In both cases, a large spread in Eu/Fe is produced at all times; even after the Eu and Fe are diluted by metal-diffusion, there exists a substantial scatter in Eu/Fe abundances.

We present the corresponding distributions of the stellar $[\text{Eu}/\text{Fe}]$ values with $[\text{Fe}/\text{H}]$ metallicity in Eris as the green contours in the bottom panels of Figure 4 (dark and light shades enclose 68 and 95 per cent of Eris’ star particles). The observational data are drawn from the samples described above, where blue symbols represent stars where α , Fe, and Eu were all measured, and orange symbols are for stars where only Eu and Fe (but not α) were reported. The most striking feature of these panels is that NS mergers are able to produce a significant scatter, even at low metallicity and early times, which agrees with the observational data. The bottom-right panel of Fig. 4 illustrates our fiducial model, which includes a prescription for mixing and a metallicity floor. Our model simultaneously provides an acceptable fit to both the $[\alpha/\text{Fe}]$ distribution and the $[\text{Eu}/\text{Fe}]$ distribution for all metallicities. Unfortunately, it is difficult to draw a direct comparison between the *distribution* of Eu/Fe values of the simulated and observed stars at low metallicity, since there are a non-negligible number of stars where Eu has not yet been detected

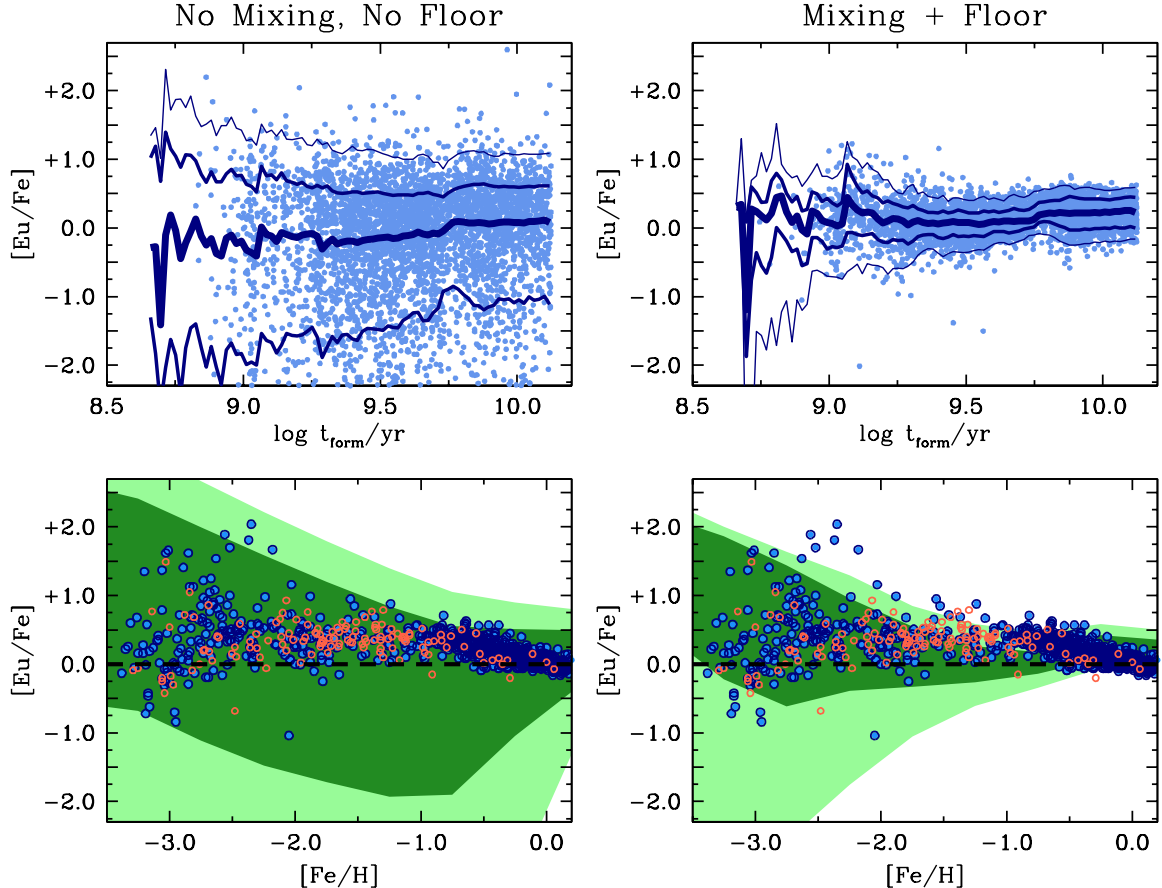


FIG. 4.— Same as Figure 3, but illustrates the chemical evolution of $[\text{Eu}/\text{Fe}]$ for our fiducial model, which corresponds to a mass ejection of $M_{\text{tr}} = 0.05 M_{\odot}$ per merger, a merger DTD that has a power law form ($P(t) \propto t^{-1}$) and a minimum merger delay-time of $t_{\text{cut}} = 100$ Myr. In this figure, orange symbols represent stars where only Eu and Fe are reported and blue symbols show stars where α , Eu and Fe are measured.

(e.g. Barklem et al. 2005; François et al. 2007; Cohen et al. 2008; Roederer et al. 2010, 2014). Nevertheless, our models suggest that the highest Eu/Fe ratios are produced at earlier times and at lower $[\text{Fe}/\text{H}]$ metallicity.

4. DISCUSSION

The density of free neutrons required for r -process synthesis points to an explosive environment (Burbidge et al. 1957). SN II have long been prime suspects although not enough is known about the detailed physics such as the explosion mechanism, the role of neutrino interactions and the equation of state in order to create realistic models that actually synthesize r -process material (e.g. Roberts et al. 2010). NS mergers offer a possible alternative to SNe as the primary r -process site (Lattimer et al. 1977). The conditions estimated to characterize the decompressed ejecta from compact binary mergers is compatible with the production of an r -process abundance pattern generally consistent with solar system matter, and in particular the third r -process peak. The most recent numerical studies of matter ejected in such relativistic mergers shows specifically that the r -process heavy nuclei are produced in solar proportion (Roberts et al. 2011; Bauswein et al. 2013; Grossman et al. 2014). The differences between these two mechanisms should be discernible in the enrichment pattern of r -process elements in the Milky Way.

Since the chemical evolution of any galaxy is intrinsically tied to its SFH, it is crucial to adopt a galaxy model that is characteristic of the Milky Way. Eris is a close analog of the Milky Way at $z = 0$, making it an ideal laboratory to study

the chemical evolution of r -process elements in the Galaxy. When we consider a simple prescription for chemical mixing, overall we find an acceptable agreement between observations and Eris for the relative production of α -capture and Fe-peak elements. By including a metallicity floor, we find that the $[\alpha/\text{Fe}]$ abundance measured for Eris is enhanced when $[\text{Fe}/\text{H}] \lesssim -1.0$, with very little scatter, in agreement with observations.

Previous studies that have investigated the chemical evolution of the r -process with NS mergers have suggested that the merger timescale needs to be relatively short (~ 1 Myr) in order for the r -process to be borne into stars with metallicities $[\text{Fe}/\text{H}] \lesssim -3.0$ (Argast et al. 2004; Matteucci et al. 2014). Our analysis, on the other hand, suggests that the chemical enrichment from NS mergers can be incorporated into stars of low $[\text{Fe}/\text{H}]$ and at early epochs even with a delay time of ~ 100 Myr. Thus, the relatively longer merger timescale argument no longer appears to be a barrier for producing r -process enhanced stars at low metallicity.

4.1. Dependence on Model Parameters

In our investigation, we have found that compact binary mergers are able to successfully produce a large dispersion in the $[\text{Eu}/\text{Fe}]$ ratios at low metallicity, which is diluted at higher metallicity due to chemical mixing. In general, the large r -process yield and the rarity of NS mergers can produce a highly varied enrichment of the r -process. We have also explored extensions to our fiducial model including: (1)

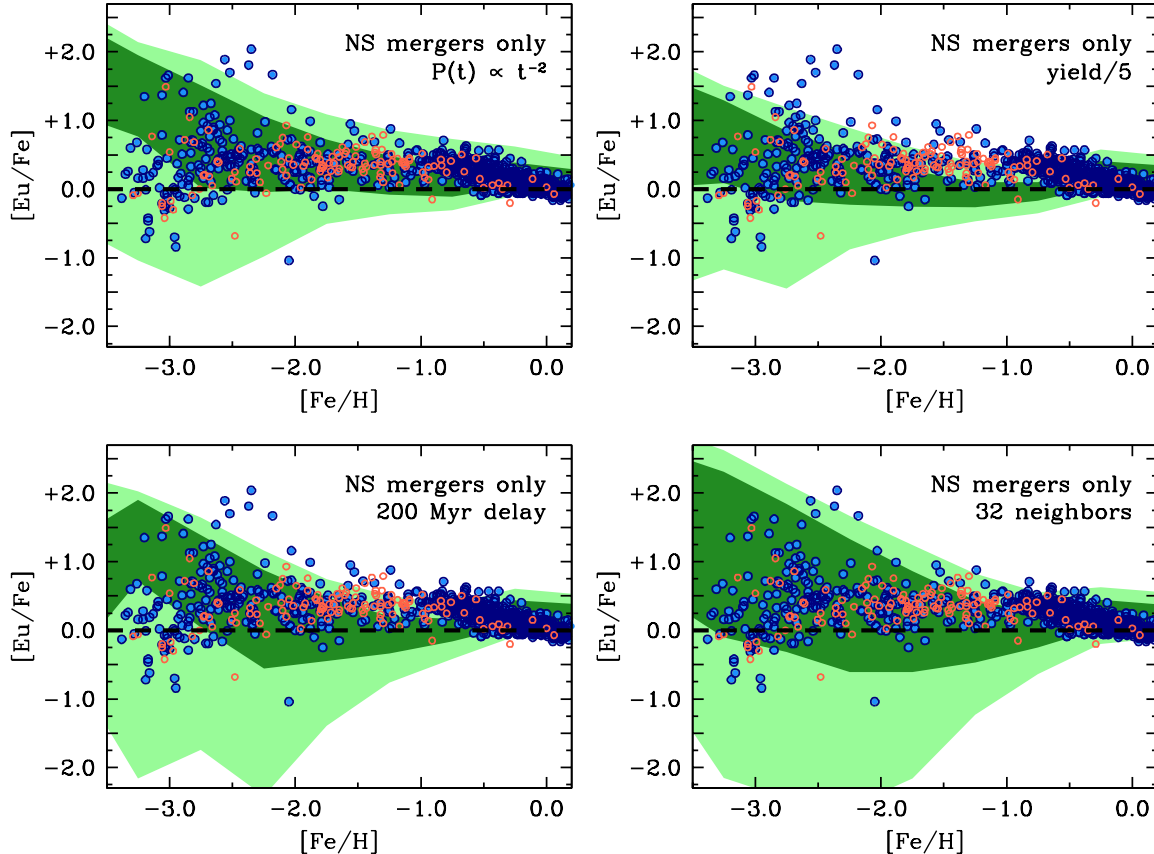


FIG. 5.— A demonstration of how the simulated $[\text{Eu}/\text{Fe}]$ contours depend on our model parameters. We make the following changes to our fiducial model: (1) change the DTD to be $P(t) \propto t^{-2}$ (top left panel); (2) increase the merger rate and reduce the yield per event by a factor of 5 (top right panel); (3) double the merger time delay to $t_{\text{cut}} = 200$ Myr (bottom left panel); and (4) less efficient mixing, by averaging 32 nearest neighbors when a star particle is formed (bottom right panel). The dark and light green contours show the $[\text{Eu}/\text{Fe}]$ distributions that respectively enclose 68 and 95 per cent of Eris’ star particles, with our mixing prescription applied. The observational data are represented by blue symbols for stars where α , Fe, and Eu were all measured, or by orange symbols for stars that only have Eu and Fe measured. The dashed line in these panels represents the solar $[\text{Eu}/\text{Fe}]$.

a DTD with $P(t) \propto t^{-2}$ (top left panel of Fig. 5); (2) increasing the frequency of mergers by a factor of five, whilst reducing the yield per event by the same amount (top right panel of Fig. 5); (3) doubling the initial time delay for mergers after a burst of star formation, to $t_{\text{cut}} = 200$ Myr (bottom left panel of Fig. 5); and (4) adopting a less efficient mixing algorithm (bottom right panel of Fig. 5). A general result of decreasing the power-law index of the DTD, is that more events will occur at earlier times (i.e. shortly after the 100 Myr delay that we have imposed). The elevated number of events at early times acts to modestly reduce the dispersion in $[\text{Eu}/\text{Fe}]$ at low metallicity. Similarly, by decreasing the Eu yield per event, the number of events are globally increased in order to match the observed Eu/O ratio in the Sun. The increased number of events also acts to slightly reduce the dispersion in $[\text{Eu}/\text{Fe}]$ at all metallicities. When we change the merger delay time to be $t_{\text{cut}} = 200$ Myr, the evolution of $[\text{Eu}/\text{Fe}]$ is qualitatively very similar to our fiducial model for $[\text{Fe}/\text{H}] \gtrsim -2.0$. However, at early times and hence lower metallicities ($[\text{Fe}/\text{H}] \lesssim -2.0$), there are subtle differences between this model extension and the fiducial model, which are largely because there are fewer lower metallicity stars being enriched with Eu. Finally, if we reduce the efficiency of mixing relative to the fiducial model, by averaging the metallicity of the 32 nearest gas particles when a star particle is born, our model provides a poorer description of the $[\text{Eu}/\text{Fe}]$ chemical evolution, particularly for

the low $[\text{Eu}/\text{Fe}]$ stars⁵.

We therefore conclude that modest variations of the model parameters for the injection history of the r -process, do not significantly alter our results – Eris displays a general correspondence with the chemical evolution of $[\text{Eu}/\text{Fe}]$ observed in the Milky Way. The choice of mixing does not significantly affect the $[\text{Eu}/\text{Fe}]$ distribution of the strongly Eu-enhanced stars, where $[\text{Eu}/\text{Fe}] \gtrsim 0.0$, and both models provide an acceptable fit to the data in this regime. The choice of mixing does, however, affect the distribution of the lowest $[\text{Eu}/\text{Fe}]$ stars. This regime is also the most poorly constrained by observations, since there are many stars where the Eu abundance has not been measured (e.g. Barklem et al. 2005; François et al. 2007; Cohen et al. 2008; Roederer et al. 2010, 2014). The level of mixing is therefore best determined by using the abundance distribution of other elements, such as the $[\alpha/\text{Fe}]$ ratio as implemented herein. We encourage future studies that consider a wider range of chemical elements to obtain a better handle on the mixing process.

4.2. Comparison with 1D Models

The chemical inhomogeneity of the interstellar medium is a key aspect of chemical evolution that can be better addressed in numerical simulations. We now explore the effect

⁵ We also note that the $[\alpha/\text{Fe}]$ chemical evolution is poorly matched with this less efficient mixing prescription.

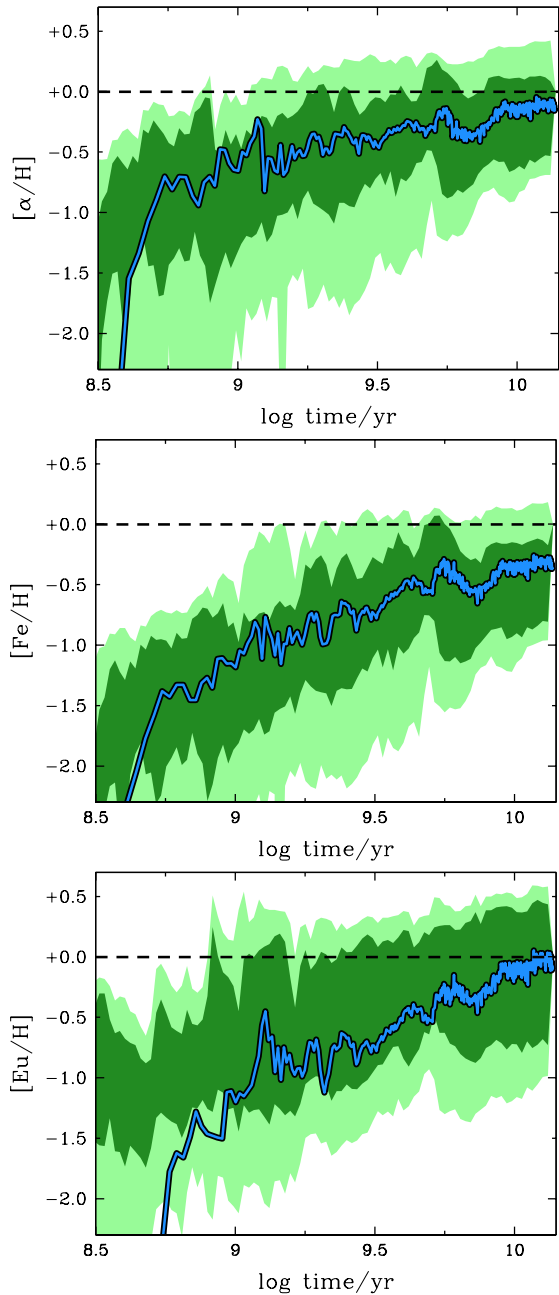


FIG. 6.— The build-up of O, Fe, and Eu in Eris after introducing a metallicity floor of $Z \sim 10^{-4}Z_{\odot}$ and a simple mixing prescription. The dark and light green regions show the 68 and 95 per cent contours that represent the metallicity distribution of stars that are born at a given time. The blue curve represents the average metallicity of the cold gas that is about to form a new generation of stars, and is therefore equivalent to a one dimensional chemical evolution model with complete chemical mixing. The significant metallicity spread of the cold gas, particularly for the high levels of Eu at early times, is not captured by a completely-mixed chemical evolution model. The horizontal dashed line shows the solar level.

of chemical inhomogeneities and metal-mixing in more detail. In particular, we consider a scenario that is similar to a 1D chemical evolution model where the metal content of all star-forming gas (i.e. gas that turns into stars at the next simulation timestep) is completely mixed before forming a new generation of stars. This assumption has been used in many analytic and semi-analytic calculations of chemical evolution. Such models provide a greater degree of physical intuition, but are unable to capture all of the relevant physical processes

that are important for galactic chemical evolution; for example, these models are not typically set in a cosmological setting. The results of our 1D experiment are shown in Figure 6, where the dark and light contours display the 68 and 95 per cent contours enclosing the chemical evolution of our fiducial model, and the single blue line illustrates the result for our 1D experiment. At late times, the centroid of both distributions agree very well, although there is clearly a very large dispersion in all of the element abundances that are considered in this work. However at early times, and hence lower metallicities, our completely-mixed chemical evolution model provides a very poor similarity to the fiducial model. Moreover, the 1D model is unable to keep track of the *dispersion* at early times (see also Argast et al. 2004), which is particularly important for Eu.

Figure 7 further illustrates the shortcomings of 1D chemical evolution models by plotting the evolution of O and Eu relative to Fe. It is evident that in the 1D models, stars with metallicities $[\text{Fe}/\text{H}] \lesssim -3.0$ cannot be formed after $\gtrsim 100$ Myrs and that most of the star-forming material in the Milky Way has reached a level of $[\text{Fe}/\text{H}] \sim -3.0$ in the $z \sim 15-20$ range. The ubiquity of Eu in stars with $[\text{Fe}/\text{H}] \lesssim -3.0$ in our cosmological simulations indicates that metal diffusion is not widespread from the sites of NS mergers until after a few Gyrs. This heavy metal flow, mixed and sheared by gas motions, remains highly anisotropic and is responsible for generating the larger-scale Eu abundance variations pervading low $[\text{Fe}/\text{H}]$ stars. The red curve in Figure 7 contrasts the model *ModINS'* from Matteucci et al. (2014) with our cosmological chemical evolution. Their *ModINS'* model shares the closest similarity to our NS merger prescription and as such provides the clearest model comparison. It is clear that 1D chemical evolution models may misrepresent the true chemical evolution of a galaxy, particularly at early times when metal mixing is not yet effective. Future studies of detailed chemical evolution in a cosmological setting (e.g. Kobayashi & Nakasato 2011; Maio, Tescari, & Cooke 2015) are thus encouraged to study the properties of metal-poor gas and stars.

4.3. Comparison with van de Voort et al. (2015)

After the submission of this paper we became aware of a recent preprint (van de Voort et al. 2015), in which the authors simultaneously reached similar conclusions as presented herein regarding the role of NS mergers in Galactic r -process enrichment using the cosmological zoom-in FIRE simulation (Hopkins et al. 2014). From the parameter study by van de Voort et al. (2015), they also note that the abundance ratio and scatter of the r -process/Fe ratio at low metallicity may be sensitive to uncertainties in modelling turbulent mixing of the ISM in their simulation. In Fig. 8, we compare the chemical evolution of Eu/Fe for their fiducial model relative to ours. Both simulations appear to track the solar abundance of Eu/Fe for $[\text{Fe}/\text{H}] \gtrsim -2.0$, and exhibit a similar level of scatter. Although both simulations exhibit a large dispersion of $[\text{Eu}/\text{Fe}]$ values for $[\text{Fe}/\text{H}] \lesssim -2.0$, the centroid of the two simulations shows an opposite evolution, which likely reflects the different model choices of Eu injection sites, numerical resolution, star formation history and feedback prescriptions between the two simulations.

Like all chemical evolution models, our conclusions may be sensitive to the assumptions of our model, such as the implementation of metal diffusion as well as the other numerical choices outlined in Section 2.1. It is nevertheless encouraging that our chemodynamical simulation with a simple, first order

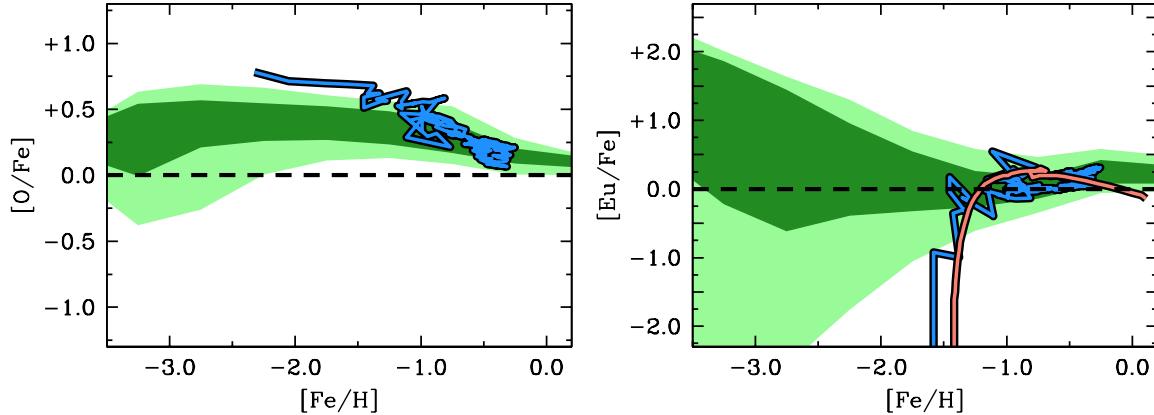


FIG. 7.— The chemical evolution of O and Eu relative to Fe for our fiducial model. The dark and light green contours enclose 68 and 95 per cent of Eris’ star particles. The blue curve shows the average abundance of the cold gas in Eris at each timestep that is about to form a new generation of stars (i.e. the equivalent of a one-dimensional chemical evolution model). Note the strong dissimilarity between the Eris results (green contours) and the completely-mixed Eris model (blue curves). The red curve illustrates model *ModINS*’ from Matteucci et al. (2014); this chemical evolution model shares the closest similarity to our NS merger prescription. The horizontal dashed black line represents the solar level of $[\text{Eu}/\text{Fe}]$.

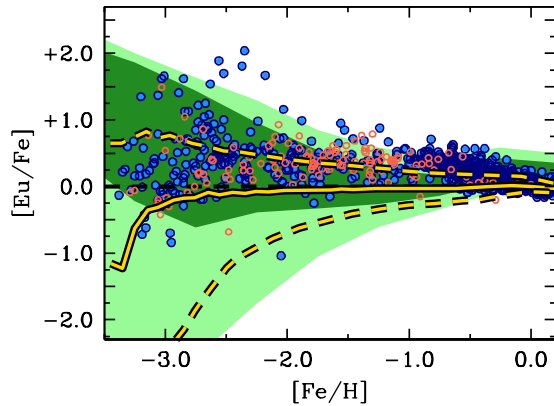


FIG. 8.— Comparing our fiducial model for the chemical evolution of Eu relative to Fe, with the recent simulations by van de Voort et al. (2015). The dark and light green contours enclose 68 and 95 per cent of Eris’ star particles. The solid yellow curve shows the distribution centroid of the fiducial model considered by van de Voort et al. (2015), and the dashed yellow contours enclose 68 per cent of their star particles. The black dashed line represents the solar level of $[\text{Eu}/\text{Fe}]$.

prescription of sub-grid metal mixing provides an acceptable agreement to the observed chemical evolution of $[\alpha/\text{Fe}]$. Future cosmological simulations that follow the chemical evolution of elements which are produced on different timescales and from a larger variety of production sites may help to elucidate some of the finer details of chemical mixing.

Our results demonstrate the importance of tracing both the dynamics and chemical evolution self-consistently in studying the origins and the evolution of r -process elements. In this regard, chemodynamic simulations are advantageous in modeling the chemical inhomogeneity in the ISM, and are

highly complementary to computationally inexpensive analytic calculations that provide a somewhat higher level of physical intuition. Future analytic and semi-analytic calculations that include a prescription of the effects of chemical inhomogeneity and mixing may provide a very useful insight into galactic chemical evolution, especially for trace elements, such as the r -process.

Whilst there need not be a single r -process production site, the current data favor a source that is either uncommon or whose yield only sporadically produced the r -process, as argued by many other authors in the past. Our study has found that NS mergers are a strong candidate as a dominant production site, even at low metallicity. Future cosmological hydrodynamic simulations with a more realistic mixing prescription, that follows a galaxy with a similar chemical evolution and SFH to that experienced by the Milky Way, are now required to investigate this problem in further detail.

We would like to thank L. Bildstein and M. Trenti for helpful discussions, and an anonymous referee for constructive comments. We gratefully acknowledge the hospitality of the Aspen Center for Physics and the DARK Cosmology Center while completing this work (NSF AST-1066293), and support from NSF (AST-1109447 and AST-0847563) and the David and Lucile Packard Foundation. R. J. C. was partially supported by NSF grant AST-1109447 during this work, and is currently supported by NASA through Hubble Fellowship grant HST-HF-51338.001-A, awarded by the Space Telescope Science Institute, which is operated by the Association of Universities for Research in Astronomy, Inc., for NASA, under contract NAS5-26555. P.M. acknowledges support by NSF grant OIA-112445329745 and NASA grant NNX12AF87G.

REFERENCES

- Abadie J., et al., 2010, *CQGra*, 27, 173001
 Argast D., Samland M., Thielemann F.-K., Qian Y.-Z., 2004, *A&A*, 416, 997
 Asplund M., Grevesse N., Sauval A. J., Scott P., 2009, *ARA&A*, 47, 481
 Barklem P. S., et al., 2005, *A&A*, 439, 129
 Bauswein, A., Goriely, S., & Janka, H.-T. 2013, *ApJ*, 773, 78
 Behroozi, P. S., Ramirez-Ruiz, E., & Fryer, C. L. 2014, arXiv:1401.7986
 Belczynski K., Perna R., Bulik T., Kalogera V., Ivanova N., Lamb D. Q., 2006, *ApJ*, 648, 1110
 Bloom J. S., Sigurdsson S., Pols O. R., 1999, *MNRAS*, 305, 763
 Brook, C. B., Stinson, G., Gibson, B. K., et al. 2014, *MNRAS*, 443, 3809
 Burbidge, E. M., Burbidge, G. R., Fowler, W. A., & Hoyle, F. 1957, *Reviews of Modern Physics*, 29, 547
 Cayrel R., et al., 2004, *A&A*, 416, 1117
 Cescutti, G., Chiappini, C., Hirschi, R., Meynet, G., & Frischknecht, U. 2013, *A&A*, 553, A51
 Cescutti G., Chiappini C., 2014, *A&A*, 565, A51
 Cohen J. G., et al., 2004, *ApJ*, 612, 1107
 Cohen, J. G., Christlieb, N., McWilliam, A., et al. 2008, *ApJ*, 672, 320
 Cowan, J. J., & Thielemann, F.-K. 2004, *Physics Today*, 57, 47
 Cowan, J. J., & Sneden, C. 2006, *Nature*, 440, 1151

- Fulbright J. P., 2000, *AJ*, 120, 1841
- Few, C. G., Courty, S., Gibson, B. K., et al. 2012, *MNRAS*, 424, L11
- Few, C. G., Courty, S., Gibson, B. K., Michel-Dansac, L., & Calura, F. 2014, *MNRAS*, 444, 3845
- Fields, B. D., Truran, J. W., & Cowan, J. J. 2002, *ApJ*, 575, 845
- François, P., Depagne, E., Hill, V., et al. 2007, *A&A*, 476, 935
- Freiburghaus, C., Rosswog, S., & Thielemann, F.-K. 1999, *ApJ*, 525, L121
- Fryer, C. L., Woosley, S. E., & Hartmann, D. H. 1999, *ApJ*, 526, 152
- Greif T. H., Glover S. C. O., Bromm V., Klessen R. S., 2009, *MNRAS*, 392, 1381
- Grossman, D., Korobkin, O., Rosswog, S., & Piran, T. 2014, *MNRAS*, 439, 757
- Guedes J., Callegari S., Madau P., Mayer L., 2011, *ApJ*, 742, 76
- Haardt F., Madau P., 1996, *ApJ*, 461, 20
- Heger A., Woosley S. E., 2010, *ApJ*, 724, 341
- Hopkins, P. F., Kereš, D., Oñorbe, J., et al. 2014, *MNRAS*, 445, 581
- Just, O., Bauswein, A., Ardevol Pulpillo, R., Goriely, S., & Janka, H.-T. 2014, arXiv:1406.2687
- Kalogera, V., Narayan, R., Spergel, D. N., & Taylor, J. H. 2001, *ApJ*, 556, 340
- Kawata, D., & Gibson, B. K. 2003, *MNRAS*, 340, 908
- Kelley, L. Z., Ramirez-Ruiz, E., Zemp, M., Diemand, J., & Mandel, I. 2010, *ApJ*, 725, L91
- Kennicutt R. C., Jr., Tamblyn P., Congdon C. E., 1994, *ApJ*, 435, 22
- Kobayashi, C., & Nakasato, N. 2011, *ApJ*, 729, 16
- Kroupa P., Tout C. A., Gilmore G., 1993, *MNRAS*, 262, 545
- Krumholz, M. R., & Gnedin, N. Y. 2011, *ApJ*, 729, 36
- Kuhlen, M., Madau, P., & Krumholz, M. R. 2013, *ApJ*, 776, 34
- Lattimer, J. M., & Schramm, D. N. 1974, *ApJ*, 192, L145
- Limongi M., Chieffi A., 2012, *ApJS*, 199, 38
- Lattimer, J. M., Mackie, F., Ravenhall, D. G., & Schramm, D. N. 1977, *ApJ*, 213, 225
- Maio U., Tescari E., Cooke R. J., 2015, *MNRAS* submitted
- Matteucci F., Romano D., Arcones A., Korobkin O., Rosswog S., 2014, *MNRAS*, 438, 2177
- Metzger, B. D., et al. 2010, *MNRAS*, 406, 2650
- Minchev, I., Chiappini, C., & Martig, M. 2013, *A&A*, 558, AA9
- Mishenina T. V., Pignatari M., Korotin S. A., Soubiran C., Charbonnel C., Thielemann F.-K., Gorbaneva T. I., Basak N. Y., 2013, *A&A*, 552, A128
- Pagel, B. E. J. 2009, *Nucleosynthesis and Chemical Evolution of Galaxies* (2nd ed.; Cambridge: Cambridge Univ. Press)
- Pilkington, K., Few, C. G., Gibson, B. K., et al. 2012, *A&A*, 540, AA56
- Piran, T. 1992, *ApJ*, 389, L45
- Rahimi, A., Kawata, D., Allende Prieto, C., et al. 2011, *MNRAS*, 415, 1469
- Raiteri C. M., Villata M., Navarro J. F., 1996, *A&A*, 315, 105
- Ramirez-Ruiz, E., Trenti, M., MacLeod, M., et al. 2014, arXiv:1410.3467
- Reddy B. E., Tomkin J., Lambert D. L., Allende Prieto C., 2003, *MNRAS*, 340, 304
- Reddy, B. E., Lambert, D. L., & Allende Prieto, C. 2006, *MNRAS*, 367, 1329
- Roberts, L. F., Woosley, S. E., & Hoffman, R. D. 2010, *ApJ*, 722, 954
- Roberts, L. F., Kasen, D., Lee, W. H., & Ramirez-Ruiz, E. 2011, *ApJ*, 736, L21
- Roederer, I. U., Cowan, J. J., Karakas, A. I., et al. 2010, *ApJ*, 724, 975
- Roederer I. U., Preston G. W., Thompson I. B., Shectman S. A., Sneden C., Burley G. S., Kelso D. D., 2014, *AJ*, 147, 136
- Rosswog, S., Liebendörfer, M., Thielemann, F.-K., Davies, M. B., Benz, W., & Piran, T. 1999, *A&A*, 341, 499
- Shen S., Wadsley J., Stinson G., 2010, *MNRAS*, 407, 1581
- Shen S., Madau P., Guedes J., Mayer L., Prochaska J. X., Wadsley J., 2013, *ApJ*, 765, 89
- Simmerer J., Sneden C., Cowan J. J., Collier J., Woolf V. M., Lawler J. E., 2004, *ApJ*, 617, 1091
- Sneden C., Cowan J. J., Gallino R., 2008, *ARA&A*, 46, 241
- Stinson G., Seth A., Katz N., Wadsley J., Governato F., Quinn T., 2006, *MNRAS*, 373, 1074
- Takahashi, K., Witt, J., & Janka, H.-T. 1994, *A&A*, 286, 857
- Thielemann F.-K., Nomoto K., Yokoi K., 1986, *A&A*, 158, 17
- Tinsley B. M., 1979, *ApJ*, 229, 1046
- Travaglio, C., Galli, D., & Burkert, A. 2001, *ApJ*, 547, 217
- Truran, J. W., Cowan, J. J., Pilachowski, C. A., & Sneden, C. 2002, *PASP*, 114, 1293
- Tsujiyama T., Shigeyama T., 2014, *ApJ*, 795, L18
- van de Voort F., Quataert E., Hopkins P. F., Kereš D., Faucher-Giguère C.-A., 2015, *MNRAS*, 447, 140
- Venn K. A., Irwin M., Shetrone M. D., Tout C. A., Hill V., Tolstoy E., 2004, *AJ*, 128, 1177
- Wadsley J. W., Stadel J., Quinn T., 2004, *NewA*, 9, 137
- Weidemann V., 1987, *A&A*, 188, 74
- Wiersma R. P. C., Schaye J., Theuns T., Dalla Vecchia C., Tornatore L., 2009, *MNRAS*, 399, 574
- Wise, J. H., Turk, M. J., Norman, M. L., & Abel, T. 2012, *ApJ*, 745, 50
- Woosley, S. E., Wilson, J. R., Mathews, G. J., Hoffman, R. D., & Meyer, B. S. 1994, *ApJ*, 433, 229
- Woosley S. E., Weaver T. A., 1995, *ApJS*, 101, 181